

# Tellurium-containing polymer coating with glutathione peroxidase mimics capability for surface modification of intravascular implants

Peichuang Li <sup>a,b</sup>, Wanhao Cai <sup>b,c</sup>, Xin Li <sup>b,d</sup>, Kebin Wang <sup>b</sup>, Lei Zhou <sup>b</sup>, Tengda Shang <sup>b</sup>, Xianmang Xu <sup>a</sup>, Yuancong Zhao <sup>b,\*</sup>, Jin Wang <sup>b,\*</sup>

<sup>a</sup> Heze Branch, Qilu University of Technology (Shandong Academy of Sciences), Biological Engineering Technology Innovation Center of Shandong Province, Heze 274000, China

<sup>b</sup> Key Laboratory of Advanced Technologies of Materials, Ministry of Education, School of Materials Science and Engineering, Southwest Jiaotong University, 610031 Chengdu, China

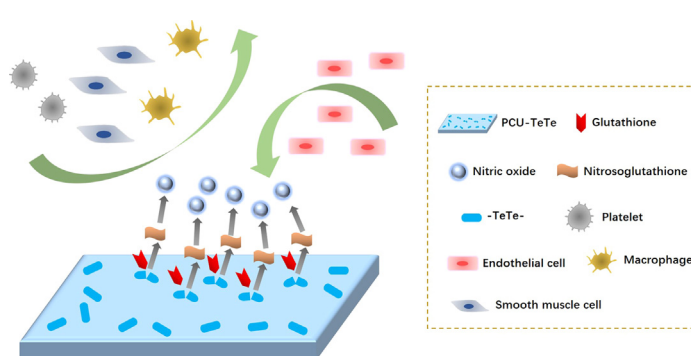
<sup>c</sup> Institute of Physical Chemistry, Albert-Ludwigs-Universität Freiburg, Albertstr. 21, 79104 Freiburg, Germany

<sup>d</sup> Department of Cardiology, Third People's Hospital of Chengdu Affiliated to Southwest Jiaotong University, Chengdu 610031, China

## HIGHLIGHTS

- A novel tellurium-functionalized polycarbonate-polyurethane is designed and synthesized by introducing ditelluride bonds.
- The tellurium-functionalized coating with glutathione peroxidase mimics capability can continuously and controllably catalyze the nitric oxide release.
- The tellurium-functionalized coating is not only beneficial for quickly building health endodermis, but also effective in inhibiting blood coagulation, endometrial hyperplasia and inflammation.

## GRAPHICAL ABSTRACT



## ARTICLE INFO

### Article history:

Received 20 January 2022

Revised 24 March 2022

Accepted 3 April 2022

Available online 6 April 2022

### Keywords:

Tellurium

Nitric oxide

Hemocompatibility

Endothelialization

Hyperplasia

## ABSTRACT

Interventional therapy as an effective method has saved millions of lives of human, in which the interventional devices (e.g. central venous catheters, vascular stent, etc.) play a crucial role. However, undesirable implantation responses including thrombus formation, inflammation, and hyperplasia is still the life-threatening to the patients. In this study, a novel tellurium-functionalized polycarbonate-polyurethane (PCU-TeTe) was designed and synthesized by introducing ditelluride bonds (Te-Te) into the molecular structure of polymer. The developed PCU-TeTe showed an excellent catalytic activity in the nitric oxide (NO) release with a rate of  $2.8 \times 10^{-10} \text{ mol} \cdot \text{cm}^{-2} \cdot \text{min}^{-1}$ , hence has multiple advanced functions in the blood environment. Both *in vitro* and *ex vivo* results of hemocompatibility showed that PCU-TeTe could substantially reduce the probability of thrombogenesis. Besides, PCU-TeTe could significantly promote endothelial cell (EC) proliferation while suppress the growth of smooth muscle cell (SMC) and macrophage (MA). Moreover, the *in vivo* results including qualitative and quantitative data (e.g. abdominal aorta hyperplasia) demonstrated that PCU-TeTe could not only promote healthy endothelialization, but also inhibit thrombus, inflammation and hyperplasia. Such tellurium-functionalized system could be a promising strategy for the design and fabrication of vascular materials or implants, especially for blood-contacting devices in the future.

© 2022 The Authors. Published by Elsevier Ltd. This is an open access article under the CC BY-NC-ND license (<http://creativecommons.org/licenses/by-nc-nd/4.0/>).

\* Corresponding authors.

E-mail addresses: [zhaoyc7320@163.com](mailto:zhaoyc7320@163.com) (Y. Zhao), [wangjin@swjtu.edu.cn](mailto:wangjin@swjtu.edu.cn) (J. Wang).

## 1. Introduction

Cardiovascular disease is one of the primary factors threatening human health [1–3]. Notably, the incidence of coronary heart disease i.e. atherosclerosis (one of the most common vascular diseases) keeps increasing in consecutive year [4]. This severe situation not only causes great suffering to patients, but also imposes serious economic burden [5]. To solve the problem, interventional therapy has been developed to an effective tool to alleviate the condition of the patients [5–7]. Among the therapies, percutaneous coronary angioplasty (PTCA) like stent implantation, has become the major for curing atherosclerosis in clinics [8–10]. However, complications such as thrombosis, inflammation and intimal hyperplasia those could lead to the in-stent restenosis (ISR) are still limiting the long-term prognosis of patients [11,12]. In particular, endothelium injury is inevitable in stenting process, which could not only trigger the aggregation and activation of platelet (i.e., thrombogenic reactions), but also result in excessive proliferation of smooth muscle cell (i.e., intimal hyperplasia) [13]. Moreover, the production of specific extracellular matrix (ECM) molecules (e.g. nitric oxide (NO)) will be also affected at the damaged site [14]. Therefore, finding an effective strategy for avoiding the ISR is very urgent.

Polymer coating on the stent [15,16] as an promising strategy has been studied and used in clinical stent research, including polylactic acid (PLA), polycaprolactone (PCL), poly(trimethylene carbonate) (PTMC) [17,18], polyurethanes (PU) [19] and etc. Among these polymers, PU is talent showing itself due to its excellent performance and wide range of structure regulation [20]. Moreover, PU is considered to be an ideal material for preparing blood-contacting implants (e.g., artificial blood vessels [21], interventional catheters [22], and implanted patches [23]). Thus, PU is expected to have a strong potential in improving the status of cardiovascular stent. However, to date commercial PU do not completely meet the complex requirements of blood environment. The main challenge is that cardiovascular stents should not only suppress adverse factors (e.g., thrombosis, inflammation, and hyperplasia), but also promote healthy tissue construction (e.g., endothelialization) [24–27]. Therefore, ideal PU material for intravascular implant environment should possess multiple biological functions. Although numerous strategies (e.g., polymer brush [28], peptide fixation, drug molecule grafting, and inert surface) have been developed to improve the biocompatibility of PU in the blood, the common modification strategies with imperfect functions often result in a high risk of ISR [13].

A new avenue for the modification of PU can be associated with NO [29,30]. NO is an endothelium relaxing factor presented in the blood, which could effectively prevent the development of atherosclerosis. By activating the cyclic guanylate monophosphate (cGMP) pathway with NO, both platelet adhesion and smooth muscle cell (SMC) proliferation can be significantly inhibited [31,32]. Moreover, NO also has a remarkable ability to defense inflammation [33] and promote endothelialization [34]. Considering the limited donor loading capacity of NO-releasing materials [35,36], we propose a strategy to mobilize regenerative NO donor i.e. endogenous S-nitrosothiols (RSNO) for the preparation of NO-regenerative materials. Inspired from the structure and function of glutathione peroxidase (GPx), covalent bonds of chalcogenide element (e.g., tellurium) were used to design novel NO-regenerative materials which can decompose RSNO to release NO [37]. Up to now, ongoing studies on NO-regenerative materials using tellurium have not been reported. Tellurium has bigger radius and weaker electro negativity in comparison with selenium. As a result, the bond energy of Te-Te is lower than that of diselenide bond (Se-Se) and makes Te-Te more sensitive under oxidation or reduction conditions

[38–40]. Thus, tellurium-functionalized polyurethane may bring light on novel NO-regenerative materials for the manufacture of vascular implants.

Based on the above analyses, a novel polycarbonate polyurethane (PCU) material was proposed as a candidate to modify blood-contacting implants in this study. As shown in Fig. 1, by mimicking physiological processes in the humoral environment involving GPx-like catalytic capability, NO will be released from the endogenous NO donor [26,37]. In the process of samples preparation, tellurium-containing compound (DHTe) as chain extender was first synthesized via reduction and then introduced into PCU molecule with classical stepwise polymerization [19]. After that, the PCU-TeTe coating was prepared on the surface of medical metal materials. Then, a series of blood compatibility tests including platelet adhesion and *ex vivo* blood experiment were performed. Besides, in order to explore cell compatibility, three kinds of blood vessel cells including endothelial cell (EC), SMC and macrophage (MA) were seeded and cultured on the samples surface. In addition, the *in vivo* biocompatibility of PCU-TeTe were assayed by subcutaneous embedding, aortic implantation of Sprague-Dawley rat, and stent implantation of New Zealand white rabbit.

## 2. Materials and methods

### 2.1. Materials and reagents

Diphenylmethane-4,4'-diisocyanate (MDI), stannous octoate, S-nitrosoglutathione (GSNO), and L-glutathione (GSH) were all received from Sigma-Aldrich. Tellurium powder and 2-bromoethyl alcohol were purchased from Aladdin Chemical Reagent Co. Ltd. (Shanghai, China) and TCI, respectively. Polycarbonatediol (PCDL) was obtained from UBE industries, Ltd. 1,4-Butylene glycol (BDO) and N,N-Dimethylacetamide (DMAc) were distilled before use.

### 2.2. Synthesis of di(1-hydroxyethyl) ditelluride and PCU-TeTe

First, 1.52 g (40.0 mmol) of sodium borohydride was dissolved into distilled water (40 mL) and then transferred into a 250 mL flask. Then, tellurium powder (2.57 g, 40.2 mmol) was added into the above sodium borohydride solution under ice bath. After the severity of the reaction decreased, the ice bath was removed and the reaction was continued under the protection of argon gas. Once the solution was clear and transparent, another portion of tellurium powder (40.0 mmol) was added into it. Subsequently, the mixture was stirred under argon atmosphere for 3 h and then warmed briefly on the steam bath to fully participate the tellurium powder in the reaction for obtaining the purplish red  $\text{Na}_2\text{Te}_2$  solution. Then, 5.03 g of 2-bromoethyl alcohol was dissolved into tetrahydrofuran (80 mL) and then injected into the above  $\text{Na}_2\text{Te}_2$  solution [41]. Subsequently, the reaction was continued for 7 h at 50 °C under the protection of argon gas. After that, ethyl acetate was poured into the final reaction mixture to extract the final product i.e. di(1-hydroxyethyl) ditelluride (DHTe, [supplementary Figure S1A](#)). Immediately, the organic layer containing DHTe was dried with anhydrous  $\text{Mg}_2\text{SO}_4$  and concentrated under vacuum. Then, column chromatography was used to purify the final product with an eluent of ethyl acetate and dichloromethane to obtain the purplish red viscous liquid DHTe (Yield: 49%).

To obtain the PCU-TeTe consisting of MDI, PCDL and DHTe, the double tellurium bond has to be introduced into the structure of the PU. Before polymerization, PCDL was dried to remove the contained moisture at 90 °C under vacuum. Then, two molar equiva-

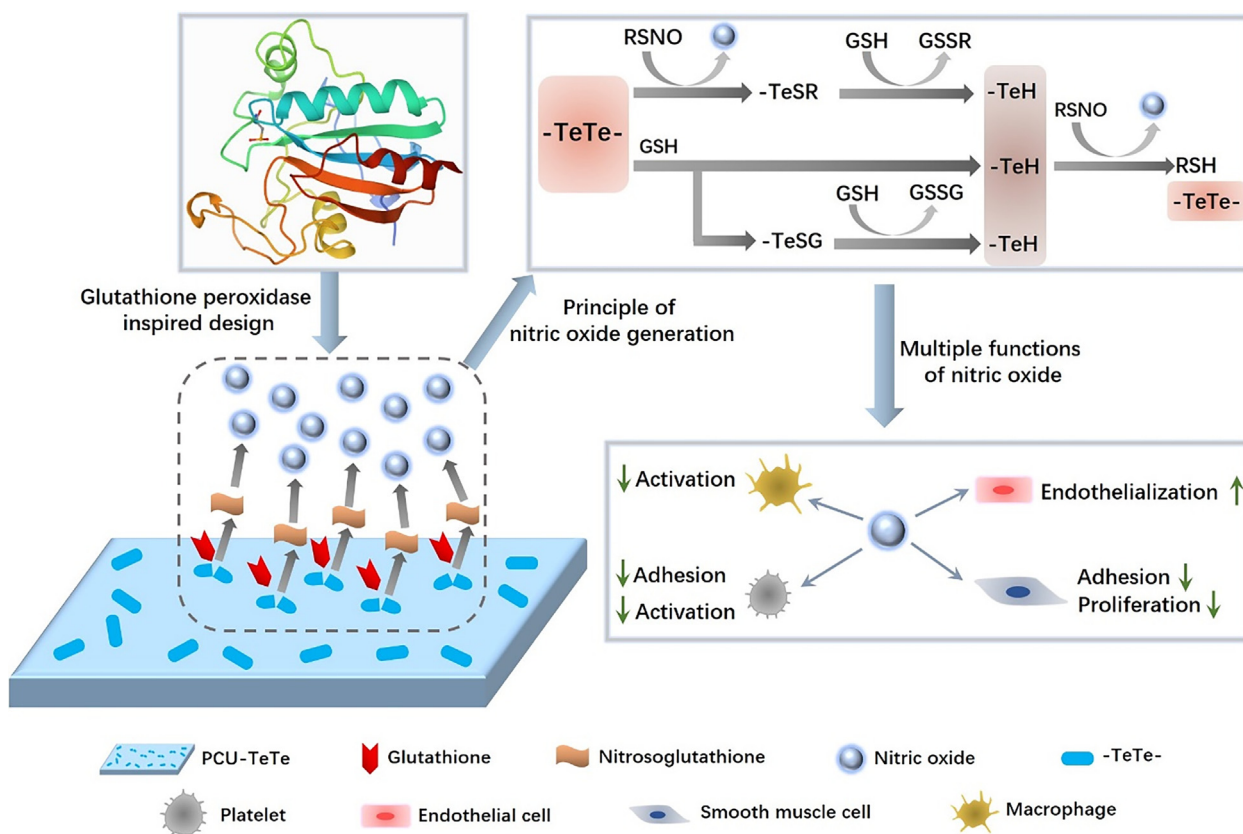


**Fig. 1.** Tellurium-functionalized PCU for the improvement of biocompatibility in blood vessel. The PCU-TeTe has multiple functions because of its catalytic capability in releasing NO. It could strongly inhibit the adhesion and activation of platelets, promote endothelialization, suppress the proliferation of SMC, and reduce the activation of MA.

lent of MDI was added into a flask containing one molar equivalent of PCDL under the protection of argon gas. After that, the mixture was allowed to react at 60 °C for 2 h. After the preparation of the pre-polymer, DMAc containing one molar equivalent of DHTe was added into the reaction. Subsequently, 0.1% of stannous octoate as catalyst was added and the chain extension was lasted for 6 h at 60 °C. Then, the final reaction solution was cooled to room temperature with the addition of methanol to precipitate the final product. Besides, PCU-BDO using BDO as chain extender was selected as the control sample (supplementary Figure S1B). Finally, the resulting products were respectively cleaned with methanol and ethanol.

### 2.3. Structure analysis and responsiveness of BHTE and PCU-TeTe

Here, Fourier transform infrared spectrometer (FTIR, NICOLET 5700) was used to obtain the information about functional groups of DHTe and PCU-TeTe, electrospray ionization mass spectrometry (ESI-MS) spectrum was used to determine the molecular weight of DHTe on a LCMS-IT-TOF apparatus, proton nuclear magnetic resonance ( $^1\text{H}$  NMR) and  $^{13}\text{C}$  NMR were used to further identify the structure composition of DHTe and PCU-TeTe on an NMR spectrometer (Bruker, 400 MHz).

Before each of the characterization, the amount of Te-Te in DHTe or PCU-TeTe was set as quantitative benchmark i.e. one equivalent. Then, dithiothreitol (DTT) as reducing agent was reacted with DHTe or PCU-TeTe, while hydrogen peroxide ( $\text{H}_2\text{O}_2$ ) as oxidizing agent was reacted with DHTe and PCU-TeTe. The

structural changes before and after reduction/oxidation were analyzed by a series of NMR spectra.

### 2.4. Preparation of PCU-BDO and PCU-TeTe coating

Stainless steel sheets (316L, the most commonly used metal for vascular implants [42]; diameter = 10 mm) were used as the substrate for preparing the polymer coating. These sheets were successively processed with polishing machine and polishing cloth to obtain the mirror-polished surface. After that, all sheets were ultrasonically cleaned three times by acetone, ethanol, and deionized water in sequence. Then, polymer solution (10%) was prepared by dissolving the moderate PCU-BDO or PCU-TeTe into tetrahydrofuran (THF). Subsequently, 316L sheets were immersed into the above polymer solution to obtain the coated surface until the solvent was evaporated thoroughly. Besides, the cross-sectional thickness of the coating was observed by SEM.

### 2.5. Catalytic release of NO

NO analyzer (NOA 280i) based on chemiluminescence was used to evaluate the real-time catalytic capacity of PCU-TeTe for releasing the NO [43]. Phosphate buffered saline (PBS, 5 mL) as reaction solution was added into the reaction vessel, mixed with NO donors consist of GSNO (10  $\mu\text{M}$ ) and GSH (10  $\mu\text{M}$ ). After the high purity nitrogen gas stream and computer signal were stabilized at 37 °C, PCU-TeTe sample was then immersed into the solution, after which the signal of NO release was captured and recorded.

## 2.6. Hemocompatibility evaluation

### 2.6.1. Platelet adhesion assay and cyclic guanosine monophosphate (cGMP) test

The acquisition and use of human blood were approved by Ethics and Welfare Committee of Southwest Jiaotong University and in accordance with the Laboratory Administration Rules. To prepare the platelet rich plasma (PRP), fresh human blood was centrifuged at 1500 rpm for 15 min. Then, NO donors consist of GSNO (10  $\mu$ M) and GSH (10  $\mu$ M) were added into PRP. Then, 100  $\mu$ L PRP was added onto each samples surface and then incubated at 37 °C for 1 h. After that, all the samples were cleaned with PBS to remove the redundant PRP. Immediately, the samples were immersed into 2.5 wt% glutaraldehyde solution to maintain the shape of adherent platelets. After that, all the samples were treated by a series of processing including dehydration, dealcoholization, critical point drying and gold sputtering. Finally, the quantity and morphology of adherent platelets were recorded by scanning electron microscopy (SEM).

Human cGMP enzyme-linked immunoassay kit purchased from Hufeng Biotechnical Co. Ltd (China) was used to estimate the cGMP level in the platelets of different samples. Before testing, each sample was soaked in 400  $\mu$ L PRP and then incubated at 37 °C for 30 min. In particular, extra joined 20  $\mu$ M GSNO and 20  $\mu$ M GSH in donor-containing groups. Then, PRP after incubation was mixed with 10% Triton-X to rupture platelet membranes with the aid of sonication. After 10 min, the mixed solution was transferred to a centrifugal tube for centrifugation (2500 rpm, 10 min). Finally, the cGMP level of the obtained supernatant was tested with ELISA.

### 2.6.2. Ex vivo coagulation test.

Animal experiments were approved by Ethics and Welfare Committee of Southwest Jiaotong University and in accordance with the Laboratory Animal Administration Rules. Adult New Zealand white rabbits with a weight of  $\sim$  4 kg each were used in the *ex vivo* coagulation test [9,27]. First, pre-cleaned 316L foils (8  $\times$  10 mm) were respectively covered with PCU-TeTe and PCU-BDO via solvent evaporation. Then, bare and modified foils were curled and placed into cardiopulmonary perfusion catheters. After that, different sides of carotid artery and external jugular vein were isolated and then connected with surgical indwelling needles. Subsequently, catheter containing foils and indwelling needles were linked together for building *ex vivo* circulation model. In the meantime, 10 mM GSNO and 10 mM GSH were injected into the blood circulation. The circulation was stopped after 1 h of coagulation test, after which the thrombus and catheter occlusion were recorded. Finally, the thrombus harvested on the foils surface was soaked into 2.5 wt% glutaraldehyde solution and then treated by dehydration, dealcoholization and weighing, and then analyzed using SEM.

## 2.7. Cytocompatibility evaluation

### 2.7.1. Vascular cells culture.

EC and SMC were cultured respectively in (Hyclone) and Dulbecco's modified Eagle medium/F12 (Hyclone) medium with fetal bovine serum (FBS, 15%) as nutrients for cell growth. The seeding density of EC and SMC was  $1.5 \times 10^4$  and  $2.0 \times 10^4$  cells/sample respectively. Culture process was carried out in the incubator containing 5% CO<sub>2</sub> at 37 °C. In donor-containing groups, NO donors (10  $\mu$ M GSNO, 10  $\mu$ M GSH) were dissolved in medium at the beginning of culture and supplemented once every 24 h. In order to observe the cell adhesion and growth status, the samples were respectively stained using 4  $\mu$ g/mL calcein-AM (Cal-AM) after 4 h, 1 day and 3 days. Then, stained cells after fixing with glutaraldehyde were pictured using fluorescent microscope (IX51,

Olympus). In particular, the viabilities of EC and SMC were detected via CCK-8 (Dojindo). Refer to the cGMP detection of platelets, after 45 min culture, a human cGMP ELISA was used to detect the cGMP level of SMC cultured on different samples.

### 2.7.2. MA culture and inflammatory factor assay.

The samples surface was seeded with mouse mononuclear macrophages (RAW 246.7) for the investigation of inflammatory cytocompatibility. High Gly medium (Hyclone) was allowed to blend with 15% FBS and then used to culture MA in a standard incubator. Before seeding, the donor-containing groups and non-donor groups were distinguished by the presence or absence of NO donors in the medium. Then, MA was seeded with a density of  $5.0 \times 10^4$  cells/sample and cultured for different times (4 h, 1 day and 3 days). Before each time point, Cal-AM was used to stain MA. Next, the samples were treated by a series of steps including rinsing with PBS, fixing with glutaraldehyde, and photographing with fluorescence microscope. Finally, the 3 days of MA culture medium was collected and then the interleukin-6 (IL-6) and tumor necrosis factor (TNF- $\alpha$ ) levels was analyzed via ELISA kits.

## 2.8. Subcutaneous implantation.

Sprague Dawley rats were chosen for evaluating the subcutaneous histocompatibility of the samples. In order to study short and long term behavior, the samples were sewn under the dorsal skin for two periods (3 weeks and 9 weeks). For self-protection, fibrous capsules would form around the implanted samples. After predetermined time, the resulting fibrous tissues were collected and then immersed into paraformaldehyde at room temperature for 3 days. Subsequently, the fibrous capsules were transferred into graded ethanol for dehydration. Then, xylene was used to saturate the fibrous tissues. After that, the resulting samples were paraffin-embedded and then sectioned with a rotary slicer. Finally, the paraffin sections were treated with hematoxylin and eosin (HE) and then pictured with a Zeiss microscope.

## 2.9. Endovascular intervention.

Twelve male Sprague Dawley rats (300–350 g) and three male adult New Zealand white rabbits (3–3.5 kg) were used in vascular implantation experiments [9]. The abdominal aortas of rats and bilateral iliac arteries of rabbits were used for samples implantation. The experimental animals were raised in a standard animal house (Basic Animal Laboratory, West China Medical College) before and after endovascular intervention, and given conventional food (SPF food) and water according to the relevant requirements of experimental animal breeding. Prior to intervention, the PCU-TeTe coating was prepared on the 316L wires and stents using ultrasonic atomizing spray, then the animals were anesthetized by injection of pentobarbital sodium.

In the wire implantation experiment, the abdominal aortas of rats were first isolated. Six rats were used in the intervention of uncoated wires (316L) and the other six were used for the coated wires (PCU-TeTe). Next, the coated and uncoated wires were implanted into the vessels. Then the vessels were sutured and gentamicin (2 mL,  $0.2 \times 10^5$  U/mL) was dropped into the abdominal cavity to reduce inflammation. After that, the skin was sewn together and penicillin (1 mL,  $1.0 \times 10^5$  U/mL) injection was performed for anti-inflammatory therapy. In the stent intervention experiment, a stent crimper was used to compress the stents on the balloon catheter. After the isolation of iliac arteries and the systemic anticoagulant treatment, the coated and uncoated stents were successively implanted into the right and left iliac arteries by percutaneous puncture angioplasty. In this experiment, three rabbits were used to set the parallel samples. Subsequently, the



rabbits were given penicillin (3 mL,  $1.0 \times 10^5$  U/mL) injection and warfarin sodium (0.6 mg, dissolved in water) feeding daily for the first 3 days.

All animals were euthanized after 30 days of implantation and the wires or stents together with the vessels were harvested. After fixation, all samples were snipped crosswise into two equal parts. Half of the samples were snipped lengthwise and then subjected to dehydration, dealcoholization, and drying. Subsequently, the dried samples were observed and recorded by SEM. The other half of the wire samples were stained and recorded via immunofluorescence method. The other half of the stent samples were used for hard tissue embedding. Finally, the embedded samples were sliced and then pictured with optical microscope.

### 3. Results and discussion

#### 3.1. Structural characterization of BHTe and PCU-TeTe

Here different methods were utilized to characterize the structure of DHTe. As shown in the FTIR spectra (Fig. 2(a)), clear peaks of methylene ( $2924\text{ cm}^{-1}$ ,  $2863\text{ cm}^{-1}$ ) and hydroxyl ( $3333\text{ cm}^{-1}$ ) groups can be observed. Sophisticated information about atoms is further offered by  $^1\text{H}$  NMR (Fig. 2(b)) that shows the peaks of protons of methylene (3.30–3.34, 3.85–3.90 ppm) and hydroxyl (2.02 ppm) groups, and  $^{13}\text{C}$  NMR (Fig. 2(c)) shows the peaks ( $64.60$  and  $8.32$  ppm) of methylene group. Moreover, the molecular weight  $M_w$  of DHTe was also identified by ESI-MS (see supplementary Figure S2). The theoretical  $M_w$  (349.8805) differs from the ESI-MS result (384.9353) by one chloride ion, in consistency with its molecular structure. These characterization results validate that DHTe was successfully synthesized.

Similar to the DHTe, the FTIR spectra of PCU-TeTe (Fig. 2(d)) shows clear peaks of methylene ( $2938$ ,  $2860\text{ cm}^{-1}$ ), secondary amine group ( $3330\text{ cm}^{-1}$ ,  $1535\text{ cm}^{-1}$ ) and MDI ( $1598\text{ cm}^{-1}$ ), while the signals of isocyanate group cannot be detected due to the complete reaction of diisocyanate. Furthermore,  $^1\text{H}$  NMR also shows

the proton peaks of PCDL (4.03, 1.57 and 1.30 ppm) and MDI (7.33, 7.08, 3.77 ppm) (Fig. 2(e)). Besides, the proton peaks of DHTe segment appeared at 4.29 ppm and 3.30 ppm. In particular, the chemical shift at 3.30 ppm overlapped with the chemical shift of water molecules remaining in dimethyl sulfoxide- $d_6$ , which can be seen from the partial amplification in Fig. 2(e). The results of FTIR and  $^1\text{H}$  NMR indicate that PCU-TeTe was successfully synthesized. In addition, the coating thickness of the sample surface (approximately  $45\text{ }\mu\text{m}$ , see Supplementary Figure S3) was detected by SEM.

#### 3.2. Redox and NO release

NMR spectra were further used here to study the oxidation and reduction responsiveness of DHTe and PCU-TeTe using  $\text{H}_2\text{O}_2$  and DTT respectively [44]. As shown in Fig. 3(a), the proton intensity of DHTe decreased remarkably after the reaction with 2 equivalent  $\text{H}_2\text{O}_2$ , and finally disappeared with the further increase of  $\text{H}_2\text{O}_2$  to 4 and 10 equivalent. At this moment, the Te-Te was oxidized and broken thoroughly. Similar results can be also observed for PCU-TeTe. As shown in Fig. 3(d), the corresponding peak of methylene in PCU-TeTe decreased with the increasing  $\text{H}_2\text{O}_2$  and finally disappeared at 4 and 10 equivalent. The result showed that PCU-TeTe can easily respond to oxide, which will relieve inflammation after the medical device implantation [45,46]. On the other hand, Te-Te has the characteristic of dynamic response in reduction environment. As shown in Fig. 3(b), (c) and (e), the absorption peaks of both  $^1\text{H}$  NMR and  $^{13}\text{C}$  NMR for DHTe and of  $^1\text{H}$  NMR for PCU-TeTe remained unchanged. These results indicated that Te-Te can be dynamically broken and reorganized in the presence of reductant, in consistency with the principle in Fig. 1. This conclusion was further validated by associated experiments of catalytic release of NO by PCU-TeTe, see latter section for the results.

NO in blood environment can effectively maintain vascular diastolic pressure and regulate the growth of vascular cells. However, dysfunction of EC in vascular lesions can lead to insufficient

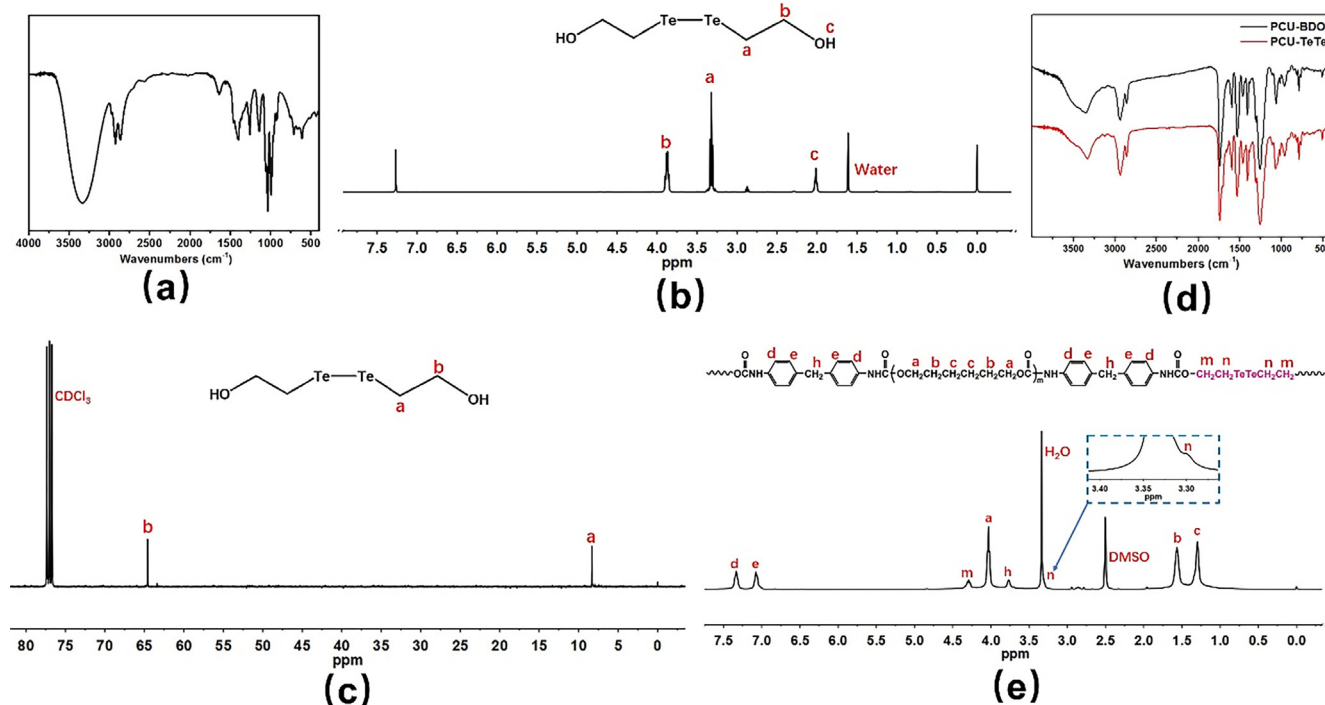
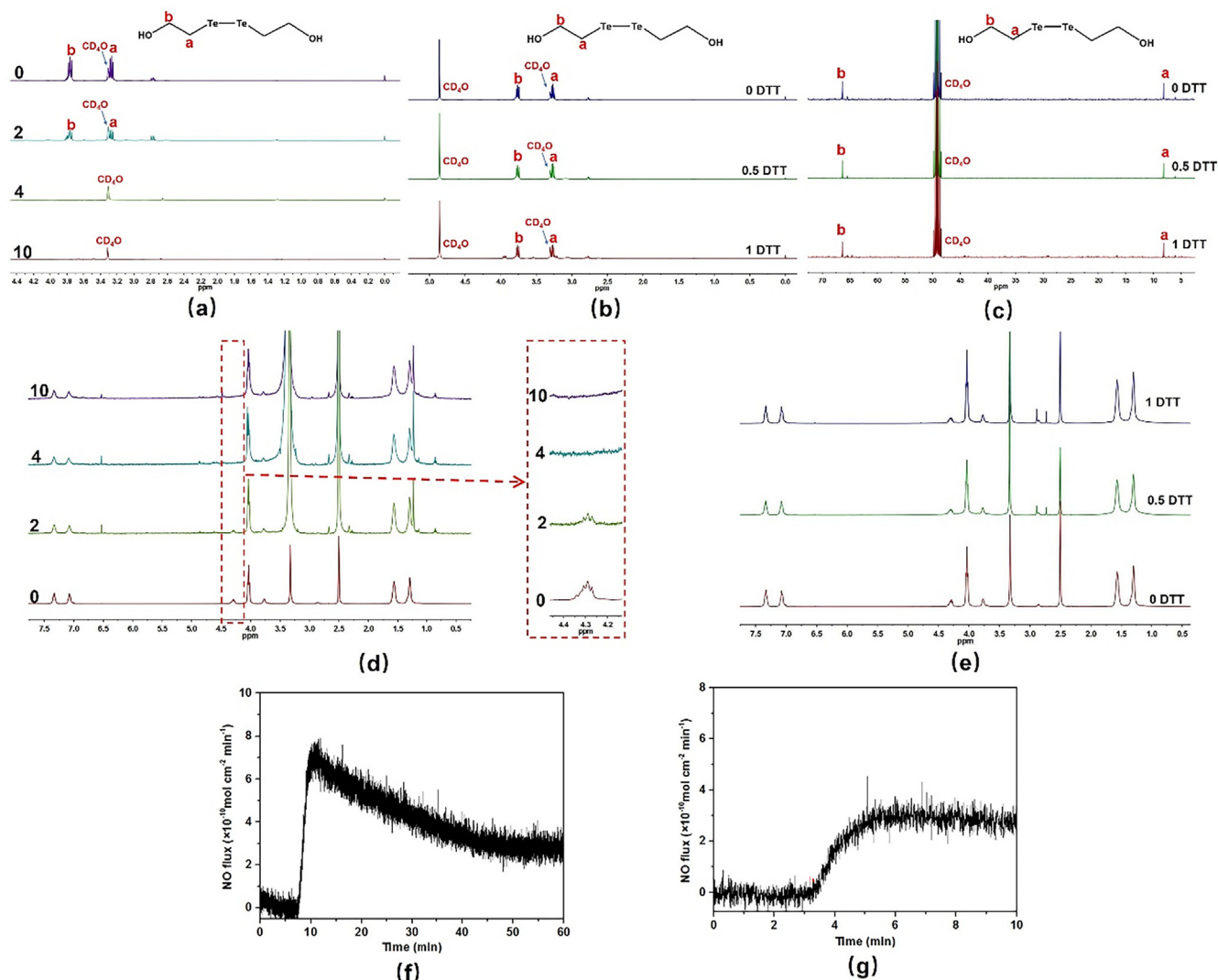


Fig. 2. Characterization of DHTe structure by (a) FTIR, (b)  $^1\text{H}$  NMR, and (c)  $^{13}\text{C}$  NMR. (d) FTIR spectra of PCU-BDO and PCU-TeTe. (e)  $^1\text{H}$  NMR spectrum of PCU-TeTe.



**Fig. 3.** (a)  $^1\text{H}$  NMR spectra after the reaction of different equivalent  $\text{H}_2\text{O}_2$  with DHTe. (b)  $^1\text{H}$  NMR and (c)  $^{13}\text{C}$  NMR spectra after the reaction of DHTe with DTT. (d)  $^1\text{H}$  NMR spectra of PCU-TeTe reacting with  $\text{H}_2\text{O}_2$  and (e) DTT. (f) Catalytic NO generation results of PCU-TeTe before and (g) after 30 days.

NO production [47]. Therefore, it is necessary to adopt effective strategies to increase the NO level in vessels. Inspired from the structure and function of GPx, the structure of Te-Te is expected to enable the decomposition of donor in a reductive environment to release NO. As can be seen from the chemiluminescence [27,43] in Fig. 3(f), the release curve remained at baseline before the sample was placed into the reaction solution, then the NO release rate increased sharply due to the sample intervention. After that, the multistage reactions between Te-Te and GSH and NO donor were in equilibrium and the release rate remained at  $2.8 \times 10^{-10} \text{ mol cm}^{-2} \text{ min}^{-1}$ , reaching the normal NO release level of EC. It can be seen that NO-regenerative materials were no longer limited by donor load (i.e. NO-releasing materials [35,36]). After the above testing, the samples were removed from the reaction solution and then protected from oxygen using argon gas for 30 days, then be studied again using chemiluminescence. Obviously, the catalytic rate of PCU-TeTe (Fig. 3(g)) did not show significant change before and after storage. This feature will ensure long-term retention of function after implantation.

### 3.3. In vitro and ex vivo hemocompatibility

Platelet behaviors including adhesion, aggregation and denaturation, which are mainly induced by non-covalent interactions such as van der Waals forces and hydrogen bonds [48,49], are not expected to occur during the service of blood interventional devices. To study the capacity of anti-adhesion of platelets, 316L, PCU-BDO and PCU-TeTe samples were cultured with platelets and then observed *via* scanning electron microscopy (SEM). As shown in Fig. 4(a), PCU-TeTe had the least number of adhered platelets among the three samples. This result was further quantified by counting results (Fig. 4(b)). Particularly, the platelet number of PCU-TeTe decreased markedly after donor addition. Besides, the SEM results (Fig. 4(a)) showed that the platelets on PCU-TeTe surface were basically nonactivated spheroids, while higher levels of activation occurred on the other two samples. These results strongly suggested that PCU-TeTe can effectively inhibit platelet adhesion and activation. The cGMP changes were also evaluated by subsequent enzyme linked immunosorbent assay (ELISA) tests.

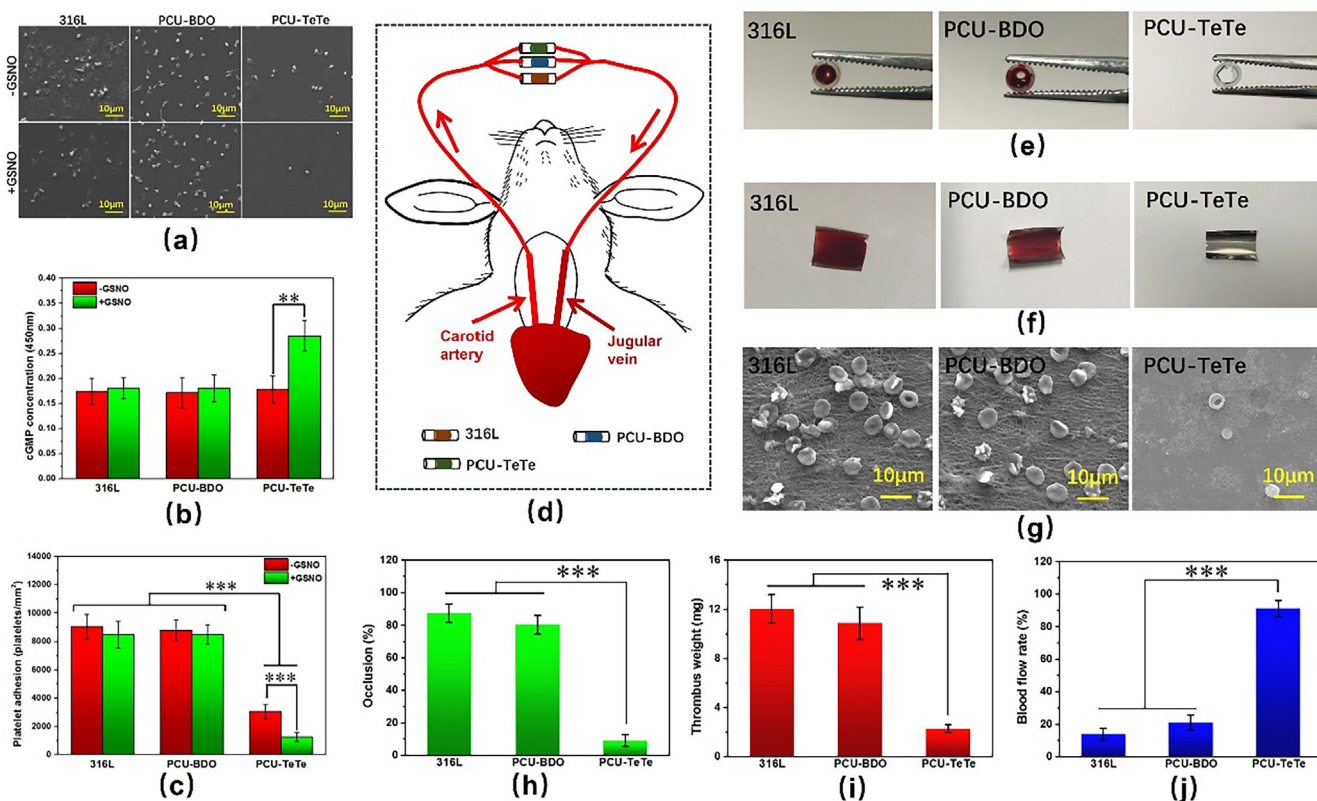


**Fig. 4.** In vitro hemocompatibility. (a) SEM images, (b) count results, and (c) cGMP levels of platelets on the surface of different samples; Further evaluation of hemocompatibility using an ex vivo circulation model. (d) Diagram of animal model. (e) Digital pictures of cross-section and (f) thrombi on the surface. (g) SEM images after circulation. (h) Occlusion ratio of sample cross-section and (i) thrombus weight results. (j) Blood flow rates at the end of evaluation (\*\* $p < 0.01$ , \*\*\* $p < 0.001$ , mean  $\pm$  SD,  $n = 5$ ).

It was found that after the addition of GSNO (S-nitrosoglutathione, NO donor), the cGMP concentration of PCU-TeTe increased markedly (Fig. 4(c)), indicating that NO had a marked effect on platelets. In contrast, the cGMP levels of PCU-BDO and 316L remained nearly constant before and after GSNO addition.

Compared with *in vitro* evaluation, live animal experiments (Fig. 4(d)) are closer to the condition of real service environment [9,27], thus can be used for the further evaluation of hemocompatibility. It was found that there was almost no obvious occlusion in PCU-TeTe sample (Fig. 4(e)), and nearly no visible thrombosis on the surface of PCU-TeTe sample (Fig. 4(f)). These digital pictures visually demonstrated that thrombosis can be impressively inhibited in PCU-TeTe samples. Subsequent SEM images (Fig. 4(g)), test samples were obtained from a single 15-minute circulation) also confirmed the excellent anticoagulant ability of PCU-TeTe: Only a small amount of blood components can be observed on the PCU-TeTe surface, while complex networks of thrombi were found on 316L and PCU-BDO. To further quantify the differences in anticoagulant capacity among different samples, multiple data including occlusion ratio, thrombus weight, and blood flow rate were analyzed. The occlusion ratio was calculated by measuring the cross-sectional diameter of the sample catheter. Thrombus weight was obtained by calculating the difference in sample weight before and after circulation. Besides, the tubes were washed with heparin solution after circulation and then simulated body fluid (5 mL) was injected into the parallel connected tubes, the time cost was recorded and compared with the initial time to indirectly obtain the blood flow rate. As shown in Fig. 4(h), (i) and (j), PCU-TeTe had the best performance in the occlusion ratio (9.0%), the lightest thrombus weight (2.2 mg) and the best antithrombotic ability with a blood flow rate of 91.0% among the three samples. These results strongly indicated that PCU-TeTe has a strong potential in the

application of blood interventional devices. In summary, by means of a series of hemocompatibility tests including platelet adhesion and activation and *ex vivo* blood experiment, PCU-TeTe was proved to have excellent anticoagulation ability.

### 3.4. EC and SMC culture

For interventional devices like vascular stents, the endothelialization after implantation is very critical, hence requires a good EC compatibility of the implanted materials. The endothelialization ability can be evaluated by studying the *in vitro* adhesion and proliferation of EC, as shown in Fig. 5 for the 316L, PCU-BDO and PCU-TeTe samples. It was found that the results of fluorescence and statistical analysis (Fig. 5(a) and (b)) of the beginning 4 h showed no significant differences among the three samples, as well as no significant differences in the same group of samples with or without NO donor. After 1-day culture, the 316L surface had the largest EC number without GSNO, but the PCU-TeTe surface after the addition of GSNO caught up with the 316L due to the promoting effect of NO on the proliferation of EC. Then after 3-day culture, the PCU-TeTe with GSNO had the highest number of EC among the three samples. Subsequent cell counting kit-8 (CCK-8) results in Fig. 5 (c) also exhibited a consistent pattern with fluorescence images and statistical analysis. In the absence of donor, there was no significant differences in 1-day CCK-8 results between PCU-TeTe and control samples. However, with the addition of GSNO and the extension of culture time, the CCK-8 value of PCU-TeTe cultured for 3 days was significantly higher than that of PCU-TeTe cultured without GSNO and also the control samples. All these results indicated that PCU-TeTe can effectively promote the growth of EC in the NO donor environment and achieve rapid endothelialization.



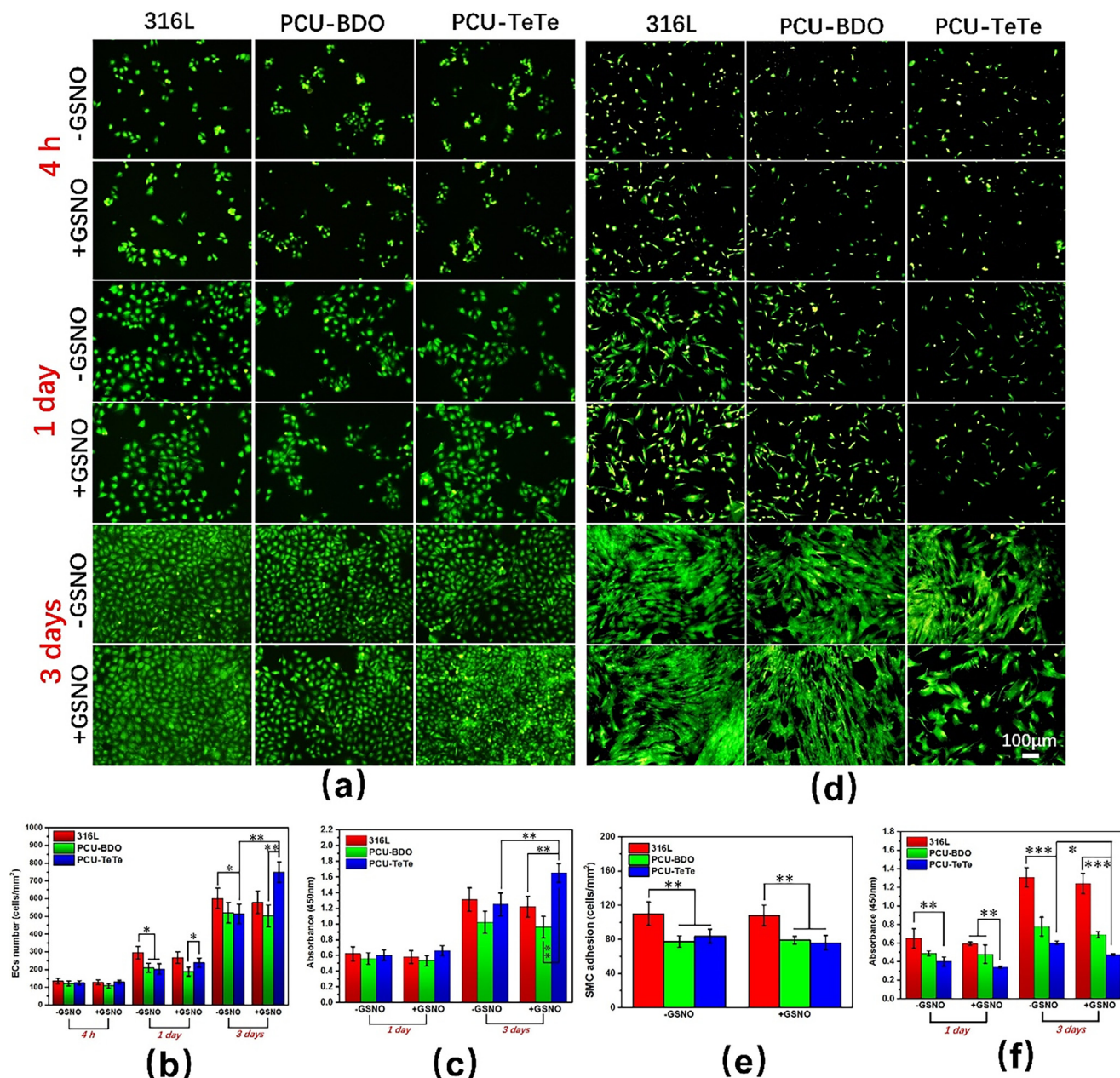


**Fig. 5.** (a) Cal-AM staining, (b) statistical analysis, and (c) CCK-8 results of EC on the surface of 316L, PCU-BDO, and PCU-TeTe. (d) Cal-AM staining, (e) 4 h adhesion analysis, and (f) cell vitality detection of SMC on different samples surface (\* $p < 0.05$ , \*\* $p < 0.01$ , mean  $\pm$  SD,  $n = 5$ ).

For cardiovascular stent materials, restenosis after implantation is mainly caused by excessive proliferation of SMC. Therefore, it is necessary to test the inhibition capacity of the proliferation of SMC for different samples. At the beginning 4 h of culture (Fig. 5(d) and (e)), 316L showed the largest number of SMC adhesion both with and without GSNO, while similar amount of SMC adhered on the surface of PCU-BDO and PCU-TeTe. A clear result can be found after the extension of culture time. After 1-day culture, the number of SMC on the PCU-TeTe was already the lowest among the three groups. After 3-day culture, the PCU-TeTe surface remained only partially covered while the other two surfaces were almost fully covered. In particular, the cell amount and CCK-8 values of PCU-TeTe (Fig. 5(f)) were further reduced after the addition of NO donor. However, the addition of GSNO did not significantly affect the control samples. Moreover, the expression level of cGMP of PCU-TeTe was increased markedly after GSNO addition (see sup-

plementary Figure S4 for details). Therefore, these results fully demonstrated that continuous and controllable catalytic performance of NO will help PCU-TeTe to inhibit SMC adhesion and proliferation.

On the whole, PCU-TeTe was found to have different compatibility of vascular cells rather than a single ability [19,50]. The growth of endothelial cell (EC) can be significantly promoted, but the proliferation of smooth muscle cell (SMC) can be strongly inhibited.

### 3.5. Subcutaneous embedding, abdominal aortic and stent implantation

Subcutaneous embedding of Sprague Dawley rats was then used to evaluate the anti-inflammatory ability of different samples. HE staining results of fibrous capsule formed at 3 and 9 weeks after



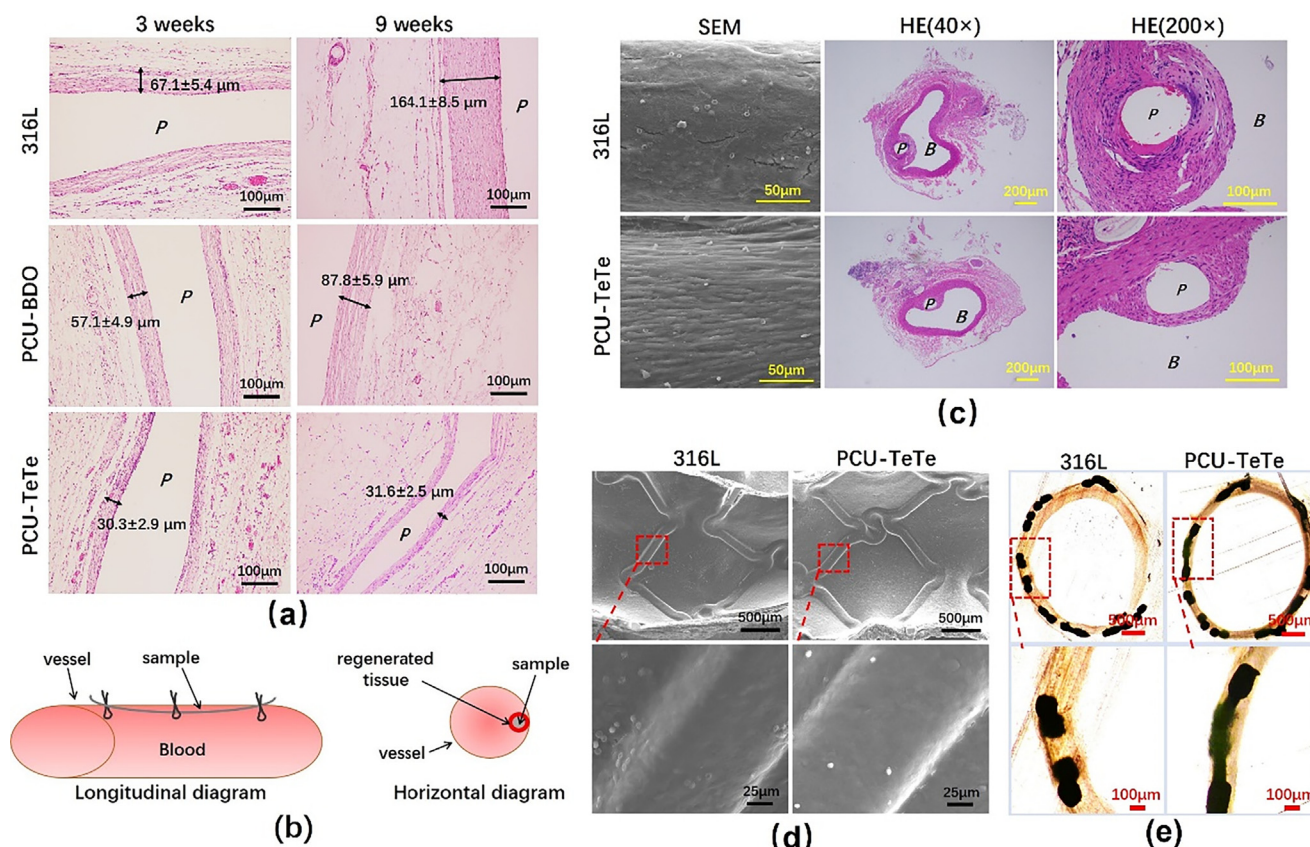


**Fig. 6.** (a) Results of subcutaneous implantation of 316L, PCU-BDO and PCU-TeTe samples in Sprague Dawley rats. (b) Polymer-coated 316L wire and bare 316L wire are implanted into the vessels. Implant diagram of the wire samples and horizontal diagram of vessels containing regenerated tissue. (c) Surface SEM images and horizontal HE staining of regenerated tissue (*B* represents blood flow, *P* represents sample sites). (d) Stent implantation results of New Zealand rabbits. SEM results of the internal surface of the iliac artery containing stent. (e) Histological pictures of hard tissue section of the iliac artery containing stent.

implantation were shown in Fig. 6(a). After 3 weeks of implantation, the thickness of fibrous capsules around PCU-BDO and 316L were  $57.1 \pm 4.9 \mu\text{m}$  and  $67.1 \pm 5.4 \mu\text{m}$ , respectively. In contrast, the thickness of fibrous capsules around PCU-TeTe were reduced to  $30.3 \pm 2.5 \mu\text{m}$ , indicating that the tissue inflammation was the lightest among the three. When the duration of implantation was extended to 9 weeks, it was found that the fibrous capsules thickness of 316L further increased to  $164.1 \pm 8.5 \mu\text{m}$ , which was due to the aggravation of inflammation caused by the continuous effect of metal ions in 316L medical stainless steel. At the same time, the fibrous capsules thickness of PCU-BDO also increased to  $87.8 \pm 5.9 \mu\text{m}$ . Notably, the fibrous capsules thickness of PCU-TeTe only slightly increased to  $31.6 \pm 2.5 \mu\text{m}$ . These results indicated that PCU-TeTe has the strongest anti-inflammatory capacity compared with control samples. Besides, the results of subcutaneous embedding were consistent with relevant results of MA culture (see Supplementary Figure S5), and the strategy of tellurium-functionalized polyurethane was effective in improving the anti-inflammatory level.

To approach a credible evaluation of the biological behavior of PCU-TeTe samples after implantation in the blood environment, the method of vascular wire implantation was performed for further analysis [18,27]. From SEM results (Fig. 6(c)), it can be seen that the endodermis on 316L surface was incomplete, and the adhesion of blood cells could also be easily recognized. By contrast, the EC on PCU-TeTe surface were not only neatly arranged, but also show a long spindle shape. In addition, there was almost no adhesion of blood cells on PCU-TeTe surface. It can be seen that the regenerated surface tissue of PCU-TeTe possess the characteristics

of healthy endodermis. For HE staining (Fig. 6(c)) of regenerated tissue, the thickness of hyperplasia around PCU-TeTe was  $47.7 \pm 1.5 \mu\text{m}$ , while the thickness of 316L was significantly thicker ( $90.5 \pm 22.7 \mu\text{m}$ ). These results indicated that the PCU-TeTe sample could effectively promote the regeneration of healthy endothelial tissue and inhibit the occurrence of thrombosis after implantation. Besides, phenotypes of MA and SMC in regenerated tissues were studied via immunofluorescence staining (see supplementary Figure S6 for details). CD 206 (a positive expression of M2-type MA) expression was more pronounced in PCU-TeTe, indicating the presence of more anti-inflammatory macrophages. For SMC, although there was no significant difference in the expression level of contractile SMC ( $\alpha$ -SMA) between the two groups, the expression level of synthetic SMC (OPN) was higher in the 316L samples. Overall, these results demonstrated that PCU-TeTe can reduce the inflammatory response of stent materials and further improve the anti-proliferation ability.

To further analyze the biocompatibility of the modified stent in blood vessels, the stent was implanted into the iliac artery of New Zealand white rabbits [9]. After reaching the predetermined implantation time, the stent and its surrounding vascular tissue were collected. After tissue fixation, SEM was first used to directly observe the internal surface of regenerated tissue. As shown in Fig. 6(d), the stent surfaces of both PCU-TeTe and 316L were covered with neointimal tissue. However, it can be discovered from the local magnified image that many blood cells were adhered to the surface of 316L, which may increase the risk of late thrombosis. In contrast, only few platelets were found on PCU-TeTe surface, and the morphology of adherent platelets was basically not

deformed. In general, consistent with the results of *in vitro* biocompatibility evaluation, the stent modified by PCU-TeTe polymer could effectively prevent thrombosis to a certain extent after implantation. Subsequent hard tissue sections were performed for observing intimal hyperplasia in different samples. After microscopic observation, histological pictures of 316L and PCU-TeTe were recorded and the results were shown in Fig. 6(e). By comparing the results before and after modification, it was observed that the hyperplasia thickness of neointima of PCU-TeTe sample were significantly thinner than that of the 316L stent. Overall, combined with the results of a series of animal experiments on Sprague Dawley rats, the above phenomenon indicated that PCU-TeTe was more conducive for inhibiting intima stenosis.

In general, the results of subcutaneous embedding indicated that the PCU-TeTe could merely provoke minimal tissue reaction. Endovascular implantations including aortic implantation of Sprague-Dawley rat and stent implantation of New Zealand white rabbit strongly suggested that this tellurium-functionalized material could realize multiple biological functions such as anti-inflammation, anti-coagulation, anti-proliferation and healthy endothelialization.

#### 4. Conclusion

In this study, tellurium-functionalized polycarbonate-polyurethane was successfully prepared and applied to the stent surface modification. The obtained PCU-TeTe coating with GPx mimics capability could continuously and controllably catalyze the NO release, hence has many advantages in the blood environments. It was found that PCU-TeTe has an excellent anticoagulation, which was validated by blood compatibility tests including platelet adhesion *in vitro* and blood circulation *ex vivo*. Besides, PCU-TeTe has a good compatibility of EC as well as a good inhibition capacity of SMC and MA. Further results from a series of animal experiments showed that PCU-TeTe is not only beneficial for quickly building health endodermis, but also effective in inhibiting blood coagulation, endometrial hyperplasia and inflammation. On the whole, the NO-releasing function endows PCU-TeTe coating with multiple biological functions compared to traditional DES coating. We anticipate that this modification strategy i.e. modified material using tellurium could be applied to blood-contacting implants in the future.

##### Authors' Contributions.

P. Li performed most experiment. X. Li, K. Wang, Lei Zhou and T. Shang contributed to the animal experiments. Y. Zhao and J. Wang directed the research. P. Li, Y. Zhao and J. Wang conceived and supervised the study and planned the experiments. P. Li, W. Cai, X. Xu, Y. Zhao, X. Li and J. Wang analyzed the data. P. Li and W. Cai discussed the mechanism, wrote and revised the manuscript.

#### Declaration of Competing Interest

The authors declare that they have no known competing financial interests or personal relationships that could have appeared to influence the work reported in this paper.

#### Acknowledgements

This work was financially supported by Natural Science Foundation of China (NSFC Project 32071328 & 81801853), Sichuan Science and Technology Program (2019YFH049 & 2020YFH0103), and Fundamental Research Funds for the Central Universities (LKPY2020-L).

#### Data Availability

All data needed to evaluate the conclusions in the paper are present in the paper and/or the [Supplementary Materials](#). Additional data related to this paper may be requested from the authors.

#### Appendix A. Supplementary material

Supplementary data to this article can be found online at <https://doi.org/10.1016/j.matdes.2022.110622>.

#### References

- [1] T.P. Baggett, S.S. Liauw, S.W. Hwang, Cardiovascular disease and homelessness, *J. Am. Coll. Cardiol.* 71 (2018) 2585–2597.
- [2] T.R. Einarson, A. Acs, C. Ludwig, U.H. Panton, Prevalence of cardiovascular disease in type 2 diabetes: a systematic literature review of scientific evidence from across the world in 2007–2017, *Cardiovasc. Diabetol.* 17 (2018) 1–19.
- [3] D. Labarthe, D.M. Lloyd-Jones, 50× 50× 50: cardiovascular health and the cardiovascular disease endgame, *Circulation* 138 (2018) 968–970.
- [4] W. Stevens, D. Peneva, J.Z. Li, L.Z. Liu, G. Liu, R. Gao, D.N. Lakdawalla, Estimating the future burden of cardiovascular disease and the value of lipid and blood pressure control therapies in China, *BMC Health Serv. Res.* 16 (1) (2016), <https://doi.org/10.1186/s12913-016-1420-8>.
- [5] L. Li, L. Yang, Y. Liao, H. Yu, Z. Liang, B. Zhang, et al., Superhydrophilic versus normal polydopamine coating: a superior and robust platform for synergistic antibacterial and antithrombotic properties, *Chem. Eng. J.* 402 (2020) 126196.
- [6] T. Nestelberger, C. Kaiser, R. Jeger, Drug-coated balloons in cardiovascular disease: benefits, challenges, and clinical applications, *Expert Opin. Drug Del.* 17 (2) (2020) 201–211.
- [7] D. Cao, R. Chandiramani, M. Chiarito, B.E. Claessen, R. Mehran, Evolution of antithrombotic therapy in patients undergoing percutaneous coronary intervention: a 40-year journey, *Eur. Heart J.* 42 (4) (2021) 339–351.
- [8] E. Gallino, S. Massey, M. Tatoulian, D. Mantovani, Plasma polymerized allylamine films deposited on 316L stainless steel for cardiovascular stent coatings, *Surf. Coat. Tech.* 205 (7) (2010) 2461–2468.
- [9] P. Gao, H. Qiu, K. Xiong, X. Li, Q. Tu, H. Wang, et al., Metal-catechol-(amine) networks for surface synergistic catalytic modification: Therapeutic gas generation and biomolecule grafting, *Biomaterials* 248 (2020) 119981.
- [10] D. Giacoppo, F. Alfonso, B.o. Xu, B.E.P.M. Claessen, T. Adriaenssens, C. Jensen, M.J. Pérez-Vizcayno, D.-Y. Kang, R. Degenhardt, L. Pleva, J. Baan, J. Cuesta, D.-W. Park, P. Kukla, P. Jiménez-Quevedo, M. Unverdorben, R. Gao, C.K. Naber, S.-J. Park, J.P.S. Henriques, A. Kastrati, R.A. Byrne, Drug-coated balloon angioplasty versus drug-eluting stent implantation in patients with coronary stent restenosis, *J. Am. Coll. Cardiol.* 75 (21) (2020) 2664–2678.
- [11] X. Chen, B. Assadsangabi, Y. Hsiang, K. Takahata, Enabling angioplasty-ready “Smart” stents to detect in-stent restenosis and occlusion, *Adv. Sci.* 5 (2018) 1700560.
- [12] D. Giacoppo, F. Alfonso, B. Xu, B.E. Claessen, T. Adriaenssens, C. Jensen, et al., Paclitaxel-coated balloon angioplasty vs. drug-eluting stenting for the treatment of coronary in-stent restenosis: a comprehensive, collaborative, individual patient data meta-analysis of 10 randomized clinical trials (DAEDALUS study), *Eur. Heart J.* 41 (2020) 3715–3728.
- [13] Y. Yang, P. Gao, J. Wang, Q. Tu, L. Bai, K. Xiong, H. Qiu, X. Zhao, M.F. Maitz, H. Wang, X. Li, Q. Zhao, Y. Xiao, N. Huang, Z. Yang, Endothelium-mimicking multifunctional coating modified cardiovascular stents via a stepwise metal-catechol-(amine) surface engineering strategy, *Research* 2020 (2020) 1–20.
- [14] N. Lyu, Z. Du, H. Qiu, P. Gao, Q. Yao, K. Xiong, et al., Mimicking the Nitric Oxide-Releasing and Glycocalyx Functions of Endothelium on Vascular Stent Surfaces, *Adv. Sci.* 7 (2020) 2002330.
- [15] R.J. de Winter, Y. Katagiri, T. Asano, K.P. Milewski, P. Lurz, P. Buszman, et al., A sirolimus-eluting bioabsorbable polymer-coated stent (MiStent) versus an everolimus-eluting durable polymer stent (Xience) after percutaneous coronary intervention (DESSOLVE III): a randomised, single-blind, multicentre, non-inferiority, phase 3 trial, *Lancet* 391 (2018) 431–440.
- [16] L.-Y. Li, L.-Y. Cui, R.-C. Zeng, S.-Q. Li, X.-B. Chen, Y. Zheng, M.B. Kannan, Advances in functionalized polymer coatings on biodegradable magnesium alloys—A review, *Acta Biomater.* 79 (2018) 23–36.
- [17] J. Wang, Y. He, M.F. Maitz, B. Collins, K. Xiong, L. Guo, et al., A surface-eroding poly (1, 3-trimethylene carbonate) coating for fully biodegradable magnesium-based stent applications: toward better biofunction, biodegradation and biocompatibility, *Acta Biomater.* 9 (2013) 8678–8689.
- [18] C. Ye, J. Wang, A. Zhao, D. He, M.F. Maitz, N. Zhou, et al., Atorvastatin eluting coating for magnesium-based stents: control of degradation and endothelialization in a microfluidic assay and in vivo, *Adv. Mater. Tech.* 5 (2020) 1900947.
- [19] P. Li, W. Cai, X. Li, K. Wang, L. Zhou, T. You, R. Wang, H. Chen, Y. Zhao, J. Wang, N. Huang, Preparation of phospholipid-based polycarbonate urethanes for potential applications of blood-contacting implants, *Regen. Biomater.* 7 (5) (2020) 491–504.
- [20] S. Wendels, L. Avérus, Biobased polyurethanes for biomedical applications, *Bioact. Mater.* 6 (4) (2021) 1083–1106.

- [21] S. Kim, S. Liu, Smart and biostable polyurethanes for long-term implants, *ACS Biomater. Sci. Eng.* 4 (2018) 1479–1490.
- [22] A.T. Stevenson, L.M. Reese, T.K. Hill, J. McGuire, A.M. Mohs, R. Shekhar, L.R. Bickford, A.R. Whittington, Fabrication and characterization of medical grade polyurethane composite catheters for near-infrared imaging, *Biomaterials* 54 (2015) 168–176.
- [23] Z.-W. Tao, S. Wu, E.M. Cosgriff-Hernandez, J.G. Jacot, Evaluation of a polyurethane-reinforced hydrogel patch in a rat right ventricle wall replacement model, *Acta Biomater.* 101 (2020) 206–218.
- [24] H. Chen, Y. Zhao, K. Xiong, J. Li, J. Chen, P. Yang, N. Huang, Multifunctional coating based on EPC-specific peptide and phospholipid polymers for potential applications in cardiovascular implants fate, *J. Mater. Chem. B* 4 (48) (2016) 7870–7881.
- [25] P. Li, Z. Luo, X. Li, R. Wang, H. Chen, Y. Zhao, et al., Preparation, evaluation and functionalization of biomimetic block copolymer coatings for potential applications in cardiovascular implants, *Appl. Surf. Sci.* 502 (2020) 144085.
- [26] X. Li, H. Qiu, P. Gao, Y. Yang, Z. Yang, N. Huang, Synergetic coordination and catecholamine chemistry for catalytic generation of nitric oxide on vascular stents, *NPG Asia Mater.* 10 (6) (2018) 482–496.
- [27] Y. Fan, Y.u. Zhang, Q. Zhao, Y. Xie, R. Luo, P. Yang, Y. Weng, Immobilization of nano Cu-MOFs with polydopamine coating for adaptable gasotransmitter generation and copper ion delivery on cardiovascular stents, *Biomaterials* 204 (2019) 36–45.
- [28] C. Lu, N. Zhou, D. Xu, Y. Tang, S. Jin, Y. Wu, J. Shen, Surface-initiated reverse atom transfer radical polymerization (SI-RATRP) for blood-compatible polyurethane substrates, *Appl. Surf. Sci.* 258 (1) (2011) 618–626.
- [29] L.-C. Xu, M.E. Meyerhoff, C.A. Siedlecki, Blood coagulation response and bacterial adhesion to biomimetic polyurethane biomaterials prepared with surface texturing and nitric oxide release, *Acta Biomater.* 84 (2019) 77–87.
- [30] M.J. Malone-Povolny, M.H. Schoenfisch, Extended nitric oxide-releasing polyurethanes via S-nitrosothiol-modified mesoporous silica nanoparticles, *ACS Appl. Mater. Interf.* 11 (13) (2019) 12216–12223.
- [31] Y.S. Do, E.Y. Kao, F. Ganaha, H. Minamiguchi, K. Sugimoto, J. Lee, et al., In-stent restenosis limitation with stent-based controlled-release nitric oxide: initial results in rabbits, *Radiology* 230 (2004) 377–382.
- [32] P. Pacher, J.S. Beckman, L. Liaudet, Nitric oxide and peroxynitrite in health and disease, *Physiol. Rev.* 87 (1) (2007) 315–424.
- [33] L. Jiang, H. Yao, X. Luo, D. Zou, C. Han, C. Tang, et al., Copper-mediated synergistic catalytic titanium dioxide nanofilm with nitric oxide generation and anti-protein fouling for enhanced hemocompatibility and inflammatory modulation, *Appl. Mater. Today* 20 (2020) 100663.
- [34] F. Kabirian, P.B. Milan, A. Zamanian, R. Heying, M. Mozafari, Nitric oxide-releasing vascular grafts: A therapeutic strategy to promote angiogenic activity and endothelium regeneration, *Acta Biomater.* 92 (2019) 82–91.
- [35] S. Yu, G. Li, R. Liu, D. Ma, W. Xue, Dendritic Fe<sub>3</sub>O<sub>4</sub>@ poly (dopamine)@PAMAM nanocomposite as controllable NO-releasing material: a synergistic photothermal and NO antibacterial study, *Adv. Funct. Mater.* 28 (2018) 1707440.
- [36] Z. Yang, Y. Yang, K. Xiong, X. Li, P. Qi, Q. Tu, F. Jing, Y. Weng, J. Wang, N. Huang, Nitric oxide producing coating mimicking endothelium function for multifunctional vascular stents, *Biomaterials* 63 (2015) 80–92.
- [37] Z. Yang, Y. Yang, K. Xiong, J. Wang, H. Lee, N. Huang, Metal-phenolic surfaces for generating therapeutic nitric oxide gas, *Chem. Mater.* 30 (15) (2018) 5220–5226.
- [38] F. Li, T. Li, W. Cao, L.u. Wang, H. Xu, Near-infrared light stimuli-responsive synergistic therapy nanoplatfoms based on the coordination of tellurium-containing block polymer and cisplatin for cancer treatment, *Biomaterials* 133 (2017) 208–218.
- [39] F. Fan, S. Gao, S. Ji, Y.u. Fu, P. Zhang, H. Xu, Gamma radiation-responsive side-chain tellurium-containing polymer for cancer therapy, *Mater. Chem. Front.* 2 (11) (2018) 2109–2115.
- [40] C. Liu, J. Xia, S. Ji, Z. Fan, H. Xu, Visible-light-induced metathesis reaction between diselenide and ditelluride, *Chem. Commun.* 55 (19) (2019) 2813–2816.
- [41] N. Ma, Y. Li, H. Xu, Z. Wang, X.i. Zhang, Dual redox responsive assemblies formed from diselenide block copolymers, *J. Am. Chem. Soc.* 132 (2) (2010) 442–443.
- [42] X. Li, P. Gao, J. Tan, K. Xiong, M.F. Maitz, C. Pan, H. Wu, Y. Chen, Z. Yang, N. Huang, Assembly of metal-phenolic/catecholamine networks for synergistically anti-inflammatory, antimicrobial, and anticoagulant coatings, *ACS Appl. Mater. Interfaces* 10 (47) (2018) 40844–40853.
- [43] P.N. Coneski, M.H. Schoenfisch, Nitric oxide release: Part III. Measurement and reporting, *Chem. Soc. Rev.* 41 (2012) 3753–3758.
- [44] S. Ji, W. Cao, Y. Yu, H. Xu, Dynamic diselenide bonds: exchange reaction induced by visible light without catalysis, *Angew. Chem. Int. Ed.* 53 (2014) 6781–6785.
- [45] J. Yao, Y. Cheng, M. Zhou, S. Zhao, S. Lin, X. Wang, J. Wu, S. Li, H. Wei, ROS scavenging Mn<sub>3</sub>O<sub>4</sub> nanozymes for in vivo anti-inflammation, *Chem. Sci.* 9 (11) (2018) 2927–2933.
- [46] L. Fan, P. Sun, Y. Huang, Z. Xu, X. Lu, J. Xi, J. Han, R. Guo, One-Pot synthesis of Fe/N-doped hollow carbon nanospheres with multienzyme mimic activities against Inflammation, *ACS Appl. Bio Mater.* 3 (2) (2020) 1147–1157.
- [47] K.-H. Park, W.J. Park, Endothelial dysfunction: clinical implications in cardiovascular disease and therapeutic approaches, *J. Korean Med. Sci.* 30 (2015) 1213–1225.
- [48] W. Cai, C. Xiao, L. Qian, S. Cui, Detecting van der Waals forces between a single polymer repeating unit and a solid surface in high vacuum, *Nano Res.* 12 (1) (2019) 57–61.
- [49] W. Cai, D. Xu, F. Zhang, J. Wei, S. Lu, L. Qian, et al., Intramolecular hydrogen bonds in a single macromolecule: Strength in high vacuum versus liquid environments, *Nano Res.* 15 (2022) 1517–1523.
- [50] D. Lv, P. Li, L. Zhou, R. Wang, H. Chen, X. Li, et al., Synthesis, evaluation of phospholipid biomimetic polycarbonate for potential cardiovascular stents coating, *React. Funct. Polym.* 163 (2021) 104897.